Efficient Circular Thresholding

Yu-Kun Lai and Paul L. Rosin

Abstract—Otsu's algorithm for thresholding images is widely used, and the computational complexity of determining the threshold from the histogram is $O(N)$ where N is the number of histogram bins. When the algorithm is adapted to *circular* rather than *linear* histograms then two thresholds are required for binary thresholding. We show that, surprisingly, it is still possible to determine the *optimal* threshold in $O(N)$ time. The efficient optimal algorithm is over 300 times faster than traditional approaches for typical histograms and is thus particularly suitable for real-time applications. We further demonstrate the usefulness of circular thresholding using the adapted Otsu criterion for various applications, including analysis of optical flow data, indoor/outdoor image classification and non-photorealistic rendering. In particular, by combining circular Otsu feature with other colour/texture features, a 96.9% correct rate is obtained for indoor/outdoor classification on the well known IITM-SCID2 dataset, outperforming the state-of-the-art result by 4.3%.

Index Terms—circular histograms, thresholding, classification, segmentation

1 Introduction

Over the last few decades many image thresholding algorithms have been proposed. These can be categorised into histogram shape based, clustering based, entropy based, object attribute based, spatial methods and local methods [1]. In 1979 Nobuyuki Otsu published a clustering based method for thresholding images that has become well known and widely used [2]. A few examples of applications using Otsu's method involve thresholding images containing: ice-covered cables [3], gas oil flow [4], sand-dust storms [5], lung CT images [6], palm prints [7], and vehicle paths [8]. Otsu proposed selecting the threshold that maximises any of the three discriminant criteria:

$$\frac{\sigma_B^2}{\sigma_W^2}, \qquad \frac{\sigma_T^2}{\sigma_W^2}, \qquad \frac{\sigma_B^2}{\sigma_T^2} \tag{1}$$

where σ_W^2, σ_B^2 and σ_T^2 are the within-class, between-class, and total variances, and showed that all three criteria will produce the same threshold. Moreover, since σ_T^2 is independent of the threshold, then σ_B^2 and $1/\sigma_W^2$ can also be used as equivalent criteria.

Compared to thresholding, more general and more powerful image segmentation algorithms have been developed. However, global thresholding algorithms like Otsu's continue to be widely used since they are well founded, simple, efficient, stable, parameter free and sufficient for many applications. Also, if more adaptive segmentation is required, then it is standard practice to modify global thresholding algorithms to operate locally.

Subsequent work has developed and extended Otsu's algorithm in various ways such as: application to multidimensional (colour) images [9], [10], application to circular histograms [11], [12], [13], expansion of the 1D intensity histogram to higher dimensions to include neighbourhood intensity information [14], [15], application to recursive thresholding [16], and improvements in computational efficiency for multiple thresholds [17], [18], [19].

This paper considers thresholding images that contain circular or cyclic values, which can arise from angular data, hue values, temporal data, etc. An example is shown in figure 1, comparing thresholding hue histograms as a linear or a circular histogram. Due to the circular nature of hues, circular thresholding gives a more consistent result regarding the content (aeroplane etc.) in the image.

There is little previous literature on thresholding circular histograms. Some examples are given in [11], [12], [13] which threshold hue images for segmenting faces, blood cells, etc. However, Tseng *et al.* [11] and Wu *et al.* [12] each describe algorithms that are both iterative and non-optimal. Dimov and Laskov [13] describe an optimal algorithm, but its computational complexity for binary thresholding is $O(N^2)$ where N is the number of histogram bins, unlike the algorithm proposed in this paper which is also optimal but only has $O(N)$ complexity. In this paper we demonstrate the usefulness of the new circular thresholding algorithm for various applications, and also show how the Otsu discriminant criterion can be used effectively for classification.

2 Circular Thresholding

We consider two methods for adapting the standard Otsu thresholding algorithm to perform circular thresholding. The first rotates the histogram appropriately, and then applies linear statistics, while the second simply replaces linear statistics with circular

• *Y. Lai and P.L. Rosin are with the School of Computer Science and Informatics, Cardiff University, UK.*
E-mail: {Yukun.Lai, Paul.Rosin}@cs.cardiff.ac.uk

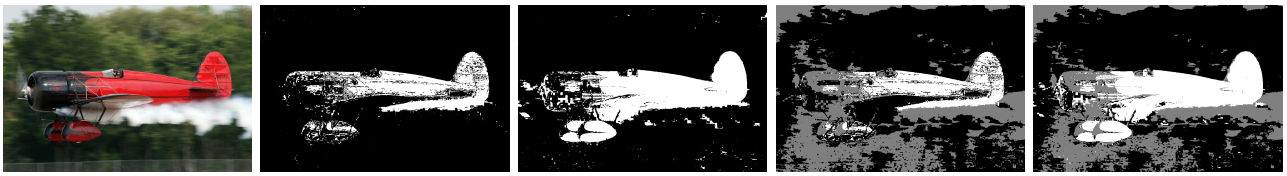

(a) (b) (c) (d) (e)

Fig. 1. Image thresholding based on hue histogram as linear or circular histogram. (a) input image; (b) two-class linear histogram; (c) two-class circular histogram; (d) three-class linear histogram; (e) three-class circular histogram.

statistics for the computation of the discriminant criterion. We start our discussion with traditional two-class thresholding due to its wide applicability, and then discuss multi-class thresholding.

2.1 Thresholding using linear statistics

The thresholding process partitions the circular histogram into two portions. Within each portion, by properly rotating the histogram, the linear statistics still apply. So the first approach rotates the histogram so as to consider all possible starting positions, and then continues to use linear statistics for each rotated histogram. The starting position and associated threshold that optimises the discriminant criterion is selected.

Unlike linear histogram thresholding, rotating the histogram will alter σ_T^2. However, once a partition is given, the circular histogram can always be rotated to obtain a linear histogram with the starting position of one portion aligned with the starting position of the linearised histogram and following [2], the identity $\sigma_T^2 = \sigma_W^2 + \sigma_B^2$ still holds for any partition. Thus both $\frac{\sigma_T^2}{\sigma_W^2}$ and $\frac{\sigma_B^2}{\sigma_T^2}$ can be re-expressed solely in terms of $\frac{\sigma_B^2}{\sigma_W^2}$: $\frac{\sigma_T^2}{\sigma_W^2} = 1 + \frac{\sigma_B^2}{\sigma_W^2}$ and $\frac{\sigma_B^2}{\sigma_T^2} = \frac{1}{1+\left(\frac{\sigma_B^2}{\sigma_W^2}\right)^{-1}}$, proving that all three discriminant criteria lead to identical optima.

In the linear histogram case, optimising $\frac{\sigma_B^2}{\sigma_W^2}$ is also identical to optimising σ_W^2 and σ_B^2 since σ_T^2 is constant for a linear histogram. In the circular histogram case, however the thresholds that optimise the criteria in equation (1) are generally different from σ_W^2 and σ_B^2. Experimentally we found that σ_W^2 gives better results as demonstrated by both synthetic (but representative) distributions and a dataset with ground truth (see section 4.1). Also, σ_W^2 has the advantage of easier generalisation to multi-class thresholding; details will be given in section 2.3. We thus generalise σ_W^2 (as one of the equivalent criteria in the linear case from Otsu's approach) to circular thresholding.

To find the two-class partitioning for a circular histogram, two thresholds are needed. The first is used to choose an appropriate starting point of the rotation and with each potential starting point another threshold needs to be determined to find two portions. Computing the Otsu criterion for a linear histogram has $O(N)$ complexity, where N is the number of histogram bins. This requires some appropriate incremental update to be used such that the statistics for a single partition can be computed in $O(1)$ amortised time. The direct extension of this approach to a circular histogram however takes $O(N^2)$ time as two thresholds instead of one are needed. However, we found that an *optimal* partition based on linear Otsu statistics always segments the histogram into two equal halves. By using this property, only one threshold needs to be determined, and linear time can still be achieved.

Consider a *circular* histogram with elements indexed from 1 to N with $p(x)$ representing the probability at x. Elements N and 1 are also adjacent. A portion of a circular histogram from element i to element j (both inclusive) is denoted as $i..j$. If i is larger than j, this is equivalent to $i..N \bigcup 1..j$. We further define the circular sum $\sum_{x=i}^{\circ j}$ as $\sum_{x=i}^{j}$ if $i \leq j$ and $\sum_{x=i}^{N} + \sum_{x=1}^{j}$ otherwise. We also define circular difference w.r.t. a starting position i as $a \overset{\circ}{-} b = (a-i) \mod N - (b-i) \mod N$, where $p \mod q$ gives a non-negative integer that has the remainder as p divided by q. This can be considered as measuring the difference after rotating the histogram such that i becomes the first element. The following theorem and corollaries ensure optimality of the efficient algorithm (see Appendix for proofs).

Theorem 2.1. *For a circular histogram of length $N = 2n$, applying the two-class Otsu criterion (σ_W^2) using linear statistics extending to circular histograms, assume the best answer is $i..j-1$, $j..i-1$. Then, there exists a best solution, such that $|j \overset{\circ}{-} i| = n$. (Note that the starting position for $\overset{\circ}{-}$ in this case does not matter as the distance happens to be half of N.)*

Corollary 2.2. *If $p(x) > 0, \forall x$, then the* unique *best solution has each segment containing n elements.*

Corollary 2.3. *If the length of the histogram $N = 2n+1$, then there exists a best solution such that one segment contains n elements and the other contains $n+1$ elements. Moreover, if $p(x) > 0, \forall x$, then the* unique *best solution satisfies that one segment has n elements and the other has $n+1$ elements.*

The theorem and corollaries show that an *optimal*

solution to the two-class Otsu criterion (σ_W^2) using linear statistics for any histogram splits the histogram into two halves (if N is even) or has one portion containing one more element than the other (if N is odd). Further if all the bins are positive, then the unique solution satisfies this property. We can then give a simple algorithm that finds the optimal thresholds efficiently. Based on the theorem and symmetry, only the first N (if odd) or $\frac{N}{2}$ (if even) elements need to be attempted as a starting point (i) and with appropriate accumulation to calculate sums in $O(1)$ amortised time, the algorithm is $O(N)$ after obtaining the histogram, instead of $O(N^2)$, which allows real-time applications. Detailed running times are reported in section 4.6.

It has been shown that Otsu's criterion is equivalent to the maximization of the likelihood of the class distributions assuming each class has a normal distribution and the same variance [20]. Of course, an equal division of the intensity range may not always be ideal. For instance, in the simple synthetic example in figure 2a which contains two classes of equal size with normal distributions, choosing one of the optimal thresholds at a point of equal error rate yields a threshold of 185 instead of the 158 produced by Otsu's criterion applied to the circular histogram. Nevertheless, this is a limitation of the basic criterion rather than its adaptation to a circular version, since applying Otsu's algorithm to a non-circular histogram produces the almost identical result (156). In such cases it would be possible to modify Otsu's criterion to cope with close to unimodal distributions [21].

2.2 Thresholding using circular statistics

Another approach to generalise the Otsu criterion to circular histograms is to use circular statistics (mean, variance and difference).

The circular mean μ of a set of n orientation samples θ_x is defined as [22]:

$$\mu = \begin{cases} \mu' & \text{if } S > 0 \text{ and } C > 0 \\ \mu' + \pi & \text{if } C < 0 \\ \mu' + 2\pi & \text{if } S < 0 \text{ and } C > 0 \end{cases}$$

where

$$\mu' = \tan^{-1}\frac{S}{C}, \quad C = \frac{1}{n}\sum_{x=1}^{n}\cos\theta_x, \quad S = \frac{1}{n}\sum_{x=1}^{n}\sin\theta_x.$$

Also, the circular variance is calculated as $\sigma = (1-R)$, where $R = \sqrt{S^2 + C^2}$. Note that $0 \le \sigma \le 1$.

For Otsu's criterion, for a circular histogram with N bins split into two portions $i..j-1$ and $j..i-1$ (both inclusive), $p(x)$ is the probability of the histogram at x. Similar to the linear case, we have

$$\omega_1 = \sum_{x=i}^{\circ\, j-1} p(x), \omega_2 = \sum_{x=j}^{\circ\, i-1} p(x).$$

Starting from i, the numbers of elements for these portions are $n_1 = |j \mathbin{\mathring{-}} i|$, $n_2 = N - n_1$. Extending the circular statistics with probability $p(x)$ as weights, and choose $\theta_x = \frac{2\pi x}{N}$,

$$C_1 = \frac{1}{n_1}\sum_{x=i}^{\circ\, j-1} p(x)\cos\theta_x, S_1 = \frac{1}{n_1}\sum_{x=i}^{\circ\, j-1} p(x)\sin\theta_x.$$

The means μ_1, μ_2 and variances σ_1^2, σ_2^2 and the total variance σ_T^2 are defined as before, with the weighted S and C. Otsu's criteria now become

$$\sigma_W^2 = \omega_1\sigma_1^2 + \omega_2\sigma_2^2, \quad \sigma_B^2 = \omega_1\omega_2(\mu_2 \ominus \mu_1)^2,$$

where $a \ominus b = \min(|a-b|, N - |a-b|)$. However in general $\sigma_W^2 + \sigma_B^2 \neq \sigma_T^2$, thus unlike the case with linear statistics, optimising σ_W^2, σ_B^2 and $\frac{\sigma_B^2}{\sigma_W^2}$ etc. are not equivalent. Thus it does not have the nice property as with linear statistics, and also Theorem 2.1 does not hold for circular statistics. Therefore finding the optimal solution requires brute force search taking $O(N^2)$ time. We will show by experiments in section 4.2 that linear statistics often give similar results to circular statistics and thus we use linear statistics in most experiments.

2.3 Multi-class thresholding

For certain applications, it is desirable to threshold a circular histogram into multiple classes. Unfortunately the theorem cannot be generalised to the multi-class case and we follow the efficient SMAWK algorithm [19]. For N bins and C classes, the linear histogram thresholding takes $O(CN)$ time, and the optimal circular histogram thresholding can be found by taking each element as the starting element, rotating the histogram, and processing the result as a linear histogram, leading to $O(CN^2)$ time. Note that our two-class thresholding algorithm only takes $O(N)$ time, and is thus much more efficient than applying this general multi-class approach directly to two-class.

3 Applications

Circular thresholding has various applications, in particular where the distributions (histograms) are naturally circular. By using the Otsu criterion, σ_W^2 can also be obtained which provides further descriptive features for applications such as classification. We briefly describe three applications that benefit from our circular thresholding.

3.1 Analysis of optical flow data

Given a pair of images, optical flow algorithms (e.g. [23]) produce a dense field of displacement vectors showing the relationship between local regions between images. When the optical flow vector directions are histogrammed, circular thresholding gives reasonable separation of different directions. More robust results can be obtained by combining circular thresholding with the magnitude of vectors such that only vectors of significant magnitudes are considered, as these vectors are generally less sensitive to noise.

3.2 Indoor/outdoor image classification

Indoor/outdoor classification is a typical scene classification problem. Given an input image, the purpose is to automatically identify whether the picture is taken indoors or outdoors. Gupta *et al.* [24] used a probabilistic neural network classifier applied to a variety of colour, texture and shape image features. They also tested Payne and Singh's method [25] in which a multiresolution estimate of edge straightness is made. Classification is done by first dividing each image into 16 equal sized windows [26]. Two schemes are proposed for classifying a window: 1/ a pair of thresholds $[T_1, T_2]$ is learnt from the training set and applied to edge straightness P so that

$$\text{classification} = \begin{cases} indoor & \text{if } P > T_2 \\ outdoor & \text{if } P < T_1. \end{cases}$$

If P lies in $[T_1, T_2]$ then the window is further subdivided into four, and each subwindow is classified. The final classification is determined by the majority window class label. 2/ Alternatively a k nearest neighbour classifier is applied to edge straightness P. Pillai *et al.* [27] used estimated depth information from images as a feature for indoor/outdoor classification as outdoor scenes tend to have more uniform depth distribution. Three variants were proposed, based on the histogram ($3D_H$), $M \times M$ block average ($3D_B$) as well as average DCT coefficients of $K \times K$ overlapping windows ($3D_D$) of the logarithm of estimated relative depths. They also implemented various features including the GIST descriptor [28], a combination of seven features sets (colour distribution, entropy, DCT etc.) [29], a combination of colour and wavelet [30], the centrist descriptor [31] as well as combining these features with $3D$ features. They used Support Vector Machines (SVM) to train the model and applied it to the test data.

Our scheme also uses a multiresolution approach, and takes the original image plus versions blurred by a Gaussian filter with $\sigma = \{1, 2, 4\}$, and then the Sobel edge detector is applied. Following Gorkani and Rosalind [26] and Payne and Singh [25] the images are subdivided into 16 equal sized windows.

In each window the circular threshold was applied to the edge orientations with the edge magnitudes used as weights when constructing the histogram. The within-class variance associated with the threshold was used as a feature. More specifically, for each image the 16 variance values generated from the subwindows are sorted and concatenated to provide a feature vector (which we call the Otsu features). We also consider a standard colour histogram in hue, saturation, value (HSV) space with $4 \times 4 \times 4$ bins and Haralick co-occurrence matrix texture features [32] in both HSV colour space and grayscale intensity. For classification we use an SVM with a Radial Basis Function (RBF) kernel.

3.3 Non-photorealistic rendering

We will finally show the application of circular thresholding to non-photorealistic rendering (NPR). The monochrome method from [33] is adapted to produce artistic colour renderings that both simplify the image (by smoothing and thresholding) and retain and enhance salient detail by overlaying both black and white lines. The lines are extracted using the approach by Kang *et al.* [34] that achieves highly coherent lines by employing locally adaptive filter kernels. Connected set morphology opening and closing operations [35] are applied to the lines to further enhance their coherence. The image is converted into HSV colour space, and each channel is blurred (Gaussian kernel with $\sigma = 8$) to remove noise and simplify subsequent regions. Note that since the hue channel is circular it requires circular blurring.

Next, each of the HSV channels is thresholded into C classes. For the value channel a standard (linear) thresholding is performed. After thresholding, the $V = 0$ pixels will be black, but due to the asymmetry of HSV space, pixels with $V = 1$ will be coloured. White only occurs if $V = 1$ and $S = 0$. Therefore, in order to obtain a reasonable quantity of white pixels, near zero saturation values (using a fixed threshold of $S_T = 0.0625$) are set to zero. The standard Otsu algorithm is applied for the remaining $C-1$ saturation classes. Hue is thresholded into C classes using the circular version of the Otsu algorithm.

For the hue channel, pixels from each thresholded class are recoloured with the mean value calculated from the source hue pixels after masking out black and white pixels. The value and saturation channels are mapped to C values uniformly spread across the full range (i.e. 0 and 1 for the two-class case) for artistic effect so as to enhance colours and retain black and white in the final output. Finally, the modified HSV channels are recombined to form a base colour image which is overlaid with the lines.

4 Experimental Results and Discussions

Various experiments are performed to compare the results with different (variations of) thresholding criteria and demonstrate the efficiency and effectiveness of the proposed approach.

4.1 Comparison of different thresholding criteria

When generalising linear histogram thresholding to circular thresholding using Otsu's criteria, various approaches are possible. We compare σ_W^2, σ_B^2 and $\frac{\sigma_B^2}{\sigma_W^2}$ using linear statistics and on both synthetic distributions and dataset with ground truth.

We first use various synthetic but representative distributions, as shown in figure 2. For the histograms

in figure 2a – figure 2c σ_B^2 performs the worst; in figure 2c and figure 2d σ_W^2 selects the most appropriate thresholds. σ_W^2 consistently gives good results for all these examples.

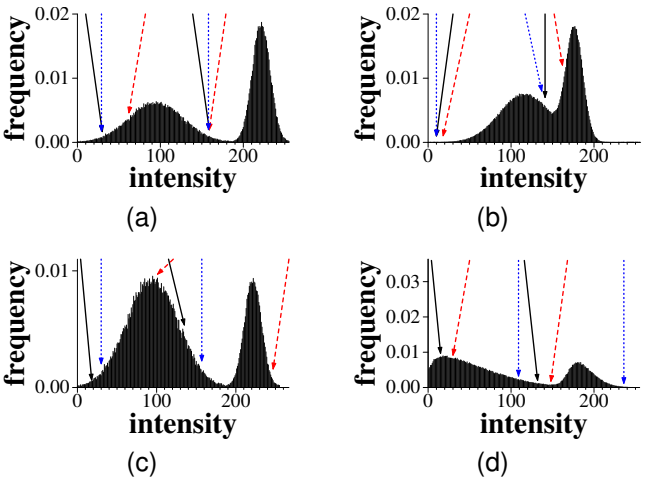

Fig. 2. Various synthetic distributions showing the circular thresholds selected according to different criteria. The solid line corresponds to any of the following: $\frac{\sigma_B^2}{\sigma_W^2}$, $\frac{\sigma_T^2}{\sigma_W^2}$, $\frac{\sigma_B^2}{\sigma_T^2}$; red dashed line: σ_B^2; blue dotted line: σ_W^2.

TABLE 1
Evaluation of document binarization on DIBCO 2009 machine printed benchmark dataset using the F-measure.

measure/image	1	2	3	4	5	mean
$\frac{\sigma_B^2}{\sigma_W^2}$	50.2	96.1	37.7	76.8	42.3	60.6
σ_B^2	35.26	51.9	33.6	17.7	32.0	34.1
σ_W^2	90.9	96.6	94.2	82.4	89.6	90.7
non-circular	90.9	96.6	96.7	82.6	89.6	91.3

We further compare various discriminant criteria considered by Otsu, by thresholding the machine printed benchmarking dataset provided at ICDAR 2009 for the Document Image Binarization Contest (DIBCO). The dataset contains 5 images of handwritten text and 5 images of printed text. We only use the 5 printed text images in our experiments because the handwritten text contains substantial degradation such as show-through, and is thus not suitable for global thresholding. Although these images do not require circular thresholding they are useful since they provide five images along with ground truth thresholded versions. Table 1 shows the results of thresholding, evaluated using the F-measure. The first three rows are circular thresholding results, using linear statistics. Since the circular thresholding can result in inverted binary images compared to the ground truth, the F-measure was also applied to the inverted result and the larger score is listed for each

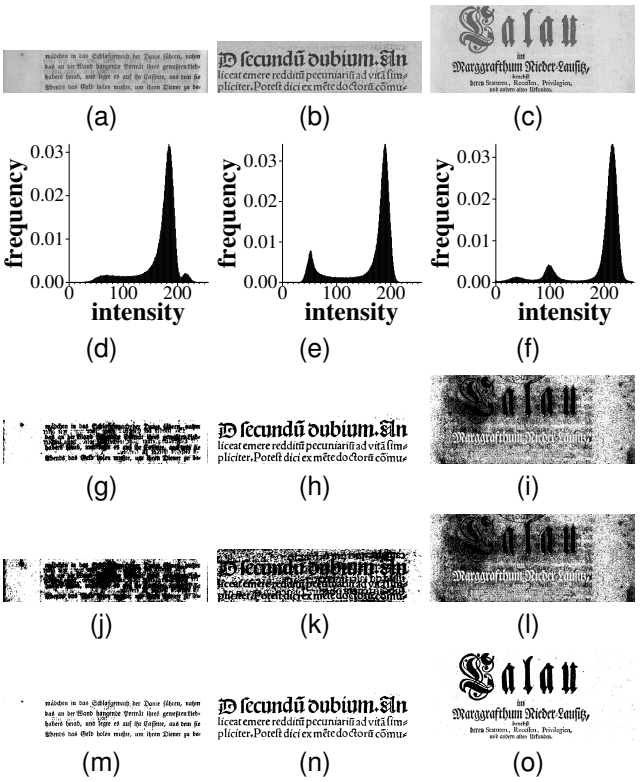

Fig. 3. Circular thresholding of images from DIBCO 2009 machine printed benchmark dataset. Column 1: P01, column 2: P02, column 3: P03. Row 1: original image, row 2: intensity histogram, row 3: circular thresholding using $\frac{\sigma_B^2}{\sigma_W^2}$, row 4: circular thresholding using σ_B^2, row 5: circular thresholding using σ_W^2.

algorithm/image. It is clear that the σ_W^2 criterion is substantially more reliable for circular thresholding than the other criteria. Its results are comparable with Otsu's non-circular thresholding, in which one threshold value (i.e. 0/256) is effectively provided in advance. Some of the threshold results are presented in figure 3. Note the different histogram shapes: almost unimodal, bimodal and trimodal.

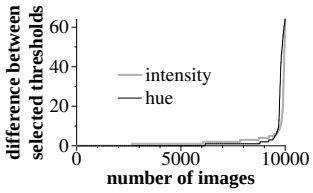

Fig. 4. Distribution of differences in thresholds selected using linear versus circular statistics.

4.2 Comparison of linear vs. circular statistics

While either linear statistics or circular statistics can be used in the discriminant criterion, the choice of statistics has little effect on the thresholding. This is demonstrated by showing the cumulative distribution

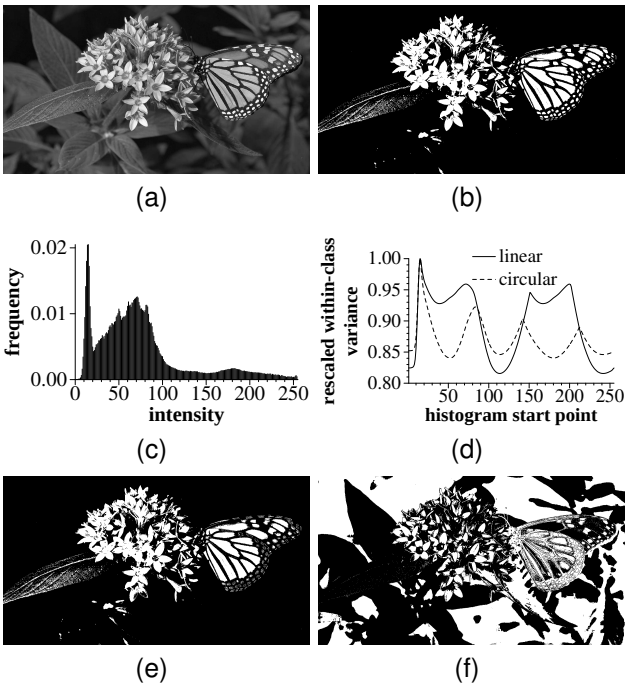

Fig. 5. An example of an image in which the thresholds selected by the algorithms using the linear (e) and circular (f) statistics produce an unusually large difference. The result using the standard (non circular histogram) Otsu criterion is shown in (b). The image's intensity histogram is shown in (c), and the within class variances as a function of threshold location are shown in (d).

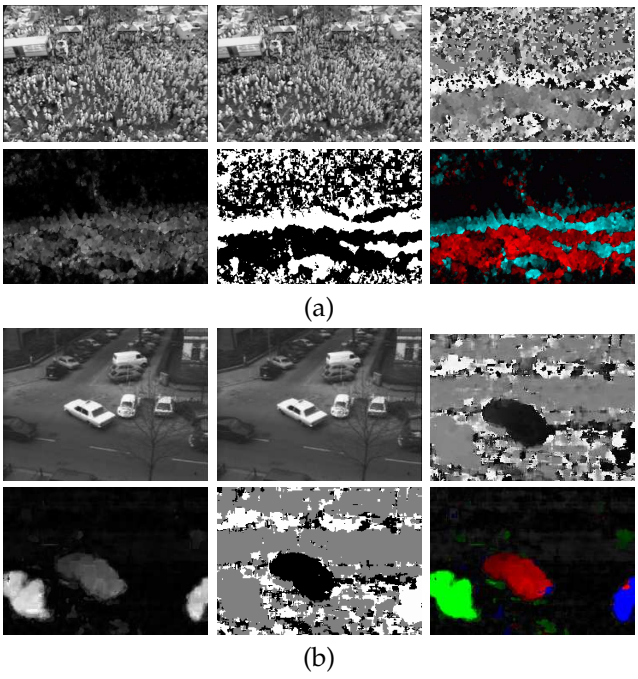

Fig. 6. Thresholding of optical flow data. a) pilgrims sequence: two frames, angle and magnitude of flow vectors, two classes after thresholding, flow vector magnitudes colour coded according to class. b) Hamburg taxi sequence: two frames, angle and magnitude of flow vectors, three classes after thresholding, flow vector magnitudes colour coded according to class.

of the differences in the thresholds selected for 10,000 randomly selected flickr images (see figure 4). We experiment on both intensity and hue histograms because hue is naturally circular but JPEG uses higher compression rates for the chromatic channels than for intensity, leading to more significant artefacts in the hue histogram. Within-class variance σ_W^2 is used for thresholding with both linear and circular statistics. For both intensity and hue histograms only a minority of images have significant differences. An example of such an extreme case is given in figure 5. From the histogram it is evident that the discriminant criterion calculated using circular statistics contains four local minima of similar magnitude evenly spread across the intensity range, all of which align closely with the (also four) corresponding local minima in the linear statistics plot. However, different global minima are selected as the threshold, leading to the large difference in results.

4.3 Analysis of optical flow data

Another illustrative example is given in figure 6 which demonstrates the application of circular thresholding to optical flow data derived from the pilgrims sequence [36] and the standard Hamburg taxi sequence using the Lucas-Kanade algorithm [23]. Circular thresholding applied to the optical flow vector directions can clearly separate objects with different moving behaviour from the background, e.g. the three cars.

4.4 Indoor/outdoor image classification

For the application of indoor/outdoor image classification, we use the IITM-SCID2 scene classification image database [24] which has been constructed to discriminate between indoor and outdoor scenes. It contains 193/200 indoor/outdoor training images and 249/260 indoor/outdoor test images. In this application, Otsu features (the within-class variance associated with the threshold) are used as a feature. We use SVM with the Radial Basis Functions kernel. Grid search and 5-fold cross validation in the training set are used to obtain the optimised parameters and the model is then applied to the test data. Default settings of LIBSVM [37] are used for this experiment. We compare our approach with state-of-the-art methods. The results are listed in table 2; we include individual features and the best combinations reported in the literature for comparison. Using the Otsu features alone, a moderate 81.1% correct rate is achieved overall. Using standard colour histogram and Haralick texture features, 91.6% correct rate is obtained, which is slightly below the best result reported in the literature

Fig. 7. Image thresholding based of hue histogram as linear or circular histogram. (a) input image; (b) two-class linear histogram; (c) two-class circular histogram; (d) three-class linear histogram; (e) three-class circular histogram.

(centrist + $3D_B$ with 92.6% correct rate). However, as the Otsu features provide rather different information from colour and texture, by combining them a 96.9% correct rate can be achieved, which is 5.3% better than using colour histogram and Haralick features alone, and 4.3% better than the best result reported in the previous literature. This test demonstrates the potential of using Otsu circular thresholding for image classification.

4.5 Application to non-photorealistic rendering

In the HSV colour model, hue is naturally circular. Using a circular histogram exploits this property and as shown in figures 1 and 7, circular thresholding of hue histograms (c, e) tends to keep the major objects (e.g. foreground/background) better separated and produces more meaningful segmentation than linear histograms (b, d).

Colour channel thresholding is applied to non-photorealistic rendering. Examples are shown in figure 8 where $C = 2$ and $C = 3$ are used for the second and third columns. The obtained images are highly stylised, emphasising the dominant colour and appear aesthetically pleasing.

4.6 Running times

We compare the efficiency of our 2-class circular thresholding algorithm with the brute force and generalised SMAWK implementations for typical bin sizes $N = 256$ and $N = 65,536$ on a computer with a 2.4 GHz Intel Core 2 Duo CPU. We run the algorithms 100 times and the average timing is reported. As shown in Table 3, our algorithm is very efficient for 2-class thresholding. For the most typical case with $N = 256$, over 300 times speedup over the brute force and the generalised SMAWK algorithms (both quadratic) is achieved. Moreover, some image sources have $N > 256$ (e.g. for medical imaging DICOM supports 16-bit data to enable differentiation of subtle differences between tissues), while derived quantities such as optical flow directions or hue can also be quanitised to $N > 256$. For $N = 65,536$, the algorithm is more than $78,000$ times faster than both approaches with quadratic complexity. Our algorithm does not generalise to cases with more than 2 classes. For

TABLE 2
Indoor/outdoor classification accuracy

Methods	Indoor	Outdoor	Total
shape [24]	63.5	66.5	65.0
colour [24]	94.0	53.5	73.3
texture [24]	94.0	86.9	90.4
colour + texture [24]	94.0	90.8	92.4
edge straightness (rule based) [25]	71.0	72.5	71.8
edge straightness (k-NN) [25]	65.6	66.5	66.1
$3D_B$ [27]	80.3	74.2	77.2
$3D_H$ [27]	63.5	78.8	71.3
$3D_D$ [27]	69.5	77.3	73.5
GIST [28]	84.7	85.2	85.0
Tao [29]	89.6	81.1	85.2
colour + wavelet [30]	87.1	83.7	85.4
centrist [31]	96.0	87.5	91.6
centrist + $3D_B$ [27]	94.4	90.9	92.6
Otsu	80.7	81.5	81.1
colour histogram + Haralick	89.6	93.5	91.6
colour histogram + Haralick + Otsu	96.4	97.3	96.9

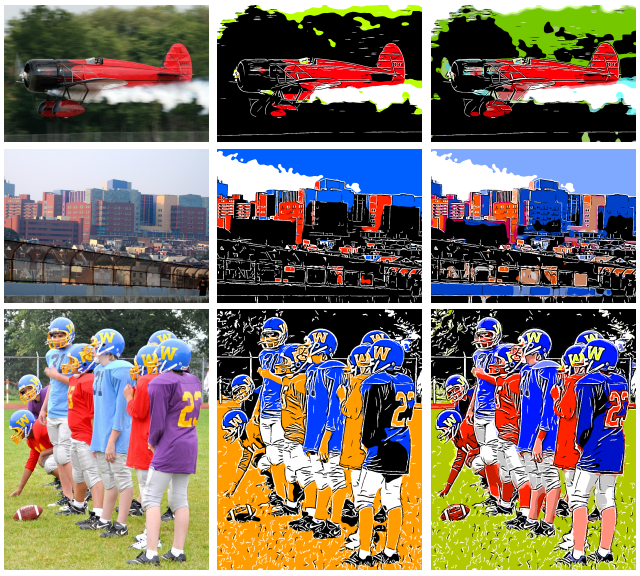

Fig. 8. Non-photorealistic rendering using thresholding. From left to right: input images, two-class thresholding and three-class thresholding.

such cases, the generalised SMAWK algorithm with $O(CN^2)$ complexity is much faster than brute force with $O(N^C)$ complexity.

5 Conclusion

In this paper we consider circular thresholding, and propose an efficient algorithm for the common two-class thresholding problem, based on the property of the Otsu criterion for the circular cases. Circular thresholding is particularly suitable for properties that are naturally circular, such as hue, orientation etc. and we demonstrate its usefulness by various applications including hue thresholding, optical flow vector thresholding, indoor/outdoor classification and non-photorealistic rendering.

References

[1] M. Sezgin and B. Sankur, "Survey over image thresholding techniques and quantitative performance evaluation," *Journal of Electronic Imaging*, vol. 13, no. 1, pp. 146–168, 2004.

[2] N. Otsu, "A threshold selection method from gray-level histograms," *IEEE Trans. SMC*, vol. 9, pp. 62–66, 1979.

[3] S. Fengjie, W. He, and F. Jieqing, "2d Otsu segmentation algorithm based on simulated annealing genetic algorithm for iced-cable images," in *Int. Forum on Information Technology and Applications*, vol. 2, 2009, pp. 600–602.

[4] X. Dailiang, J. Haifeng, H. Zhiyao, W. Baoliang, and L. Haiqing, "A new void fraction measurement method for gas-oil two-phase flow based on electrical capacitance tomography system and Otsu algorithm," in *World Congress on Intelligent Control and Automation*, vol. 4, 2004, pp. 3753–3756.

[5] K. Wei, T. Zhang, and B. He, "Detection of sand and dust storms from meris image using FE-Otsu alogrithm," in *Int. Conf. on Bioinformatics and Biomedical Engineering*, 2008, pp. 3852 –3855.

[6] W. Ying, C. Cunxi, J. Tong, and X. Xinhe, "Segmentation of regions of interest in lung ct images based on 2-d Otsu optimized by genetic algorithm," in *Chinese Control and Decision Conference*, 2009, pp. 5185 –5189.

[7] J. S. Noh and K. H. Rhee, "Palmprint identification algorithm using hu invariant moments and Otsu binarization," in *Int. Conf. on Computer and Information Science*, 2005, pp. 94–99.

[8] J. Li-Sheng, T. Lei, W. Rong-Ben, G. Lie, and C. Jiang-Wei, "An improved Otsu image segmentation algorithm for path mark detection under variable illumination," in *IEEE Intelligent Vehicles Symposium*, 2005, pp. 840 – 844.

[9] B. F. Buxton, H. Abdallahi, D. Fernandez-Reyes, and W. Jarra, "Development of an extension of the Otsu algorithm for multidimensional image segmentation of thin-film blood slides," in *Int. Conf. on Computing: Theory and Applications*, 2007, pp. 552–562.

[10] Y. Du, C. Chang, and P. Thouin, "An unsupervised approach to color video thresholding," *Optical Engineering*, vol. 43, no. 2, pp. 282–289, 2004.

[11] D.-C. Tseng, Y.-F. Li, and C.-T. Tung, "Circular histogram thresholding for color image segmentation," in *Int. Conf. on Document Analysis and Recognition*, 1995, pp. 673–676.

[12] J. Wu, P. Zeng, Y. Zhou, and C. Olivier, "A novel color image segmentation method and its application to white blood cell image analysis," in *Int Conf. Signal Processing*, vol. 2, 2006.

[13] D. Dimov and L. Laskov, "Cyclic histogram thresholding and multithresholding," in *Int. Conf. on Computer Systems and Technologies and Workshop for PhD Students in Computing*, 2009, p. 18.

[14] Q. Chen, L. Zhao, J. Lu, G. Kuang, N. Wang, and Y. Jiang, "Modified two-dimensional Otsu image segmentation algorithm and fast realisation," *IET Image Processing*, vol. 6, no. 4, pp. 426–433, 2012.

[15] N. Wang, X. Li, and X.-h. Chen, "Fast three-dimensional Otsu thresholding with shuffled frog-leaping algorithm," *Patt. Recog. Letters*, vol. 31, pp. 1809–1815, 2010.

[16] M. Cheriet, J. Said, and C. Suen, "A recursive thresholding technique for image segmentation," *IEEE Trans. IP*, vol. 7, no. 6, pp. 918–921, 1998.

[17] D.-Y. Huang and C.-H. Wang, "Optimal multi-level thresholding using a two-stage Otsu optimization approach," *Patt. Recog. Letters*, vol. 30, no. 3, pp. 275–284, 2009.

[18] B. Wu, Y. Chen, and C. Chiu, "Efficient implementation of several multilevel thresholding algorithms using a combinatorial scheme," *Int. J. of Computers and Applications*, vol. 28, no. 3, pp. 259–269, 2006.

[19] M. Luessi, M. Eichmann, G. M. Schuster, and A. K. Katsaggelos, "Framework for efficient optimal multilevel image thresholding," *Journal of Electronic Imaging*, vol. 18, pp. 013 004+, 2009.

[20] T. Kurita, N. Otsu, and N. N. Abdelmalek, "Maximum likelihood thresholding based on population mixture models," *Patt. Recog.*, vol. 25, no. 10, pp. 1231–1240, 1992.

[21] H.-F. Ng, "Automatic thresholding for defect detection," *Patt. Recog. Letters*, vol. 27, no. 14, pp. 1644 – 1649, 2006.

[22] K. Mardia and P. Jupp, *Directional Statistics*. John Wiley, 1999.

[23] B. D. Lucas and T. Kanade, "An iterative image registration technique with an application to stereo vision," in *Int. Joint Conf. on Artificial Intelligence*, 1981, pp. 674–679.

[24] L. Gupta, V. Pathangay, A. Patra, A. Dyana, and S. Das, "Indoor versus outdoor scene classification using probabilistic neural network," *EURASIP J. Adv. Sig. Proc.*, pp. 123:1–123:10, 2007.

[25] A. Payne and S. Singh, "Indoor vs. outdoor scene classification in digital photographs," *Pattern Recognition*, vol. 38, no. 10, pp. 1533–1545, 2005.

[26] M. M. Gorkani and R. W. Picard, "Texture orientation for sorting photos 'at a glance'," in *Int. Conf. Pattern Recognition ICPR*, 1994, pp. 459–464.

[27] I. Pillai, R. Satta, G. Fumera, and F. Roli, "Exploiting depth information for indoor-outdoor scene classification," in *International Conference on Image Analysis and Processing - Volume Part II*, 2011, pp. 130–139.

[28] A. Oliva and A. Torralba, "Modeling the shape of the scene: A holistic representation of the spatial envelope," *Int. J. Computer Vision*, vol. 42, no. 3, pp. 145–175, 2001.

[29] L. Tao, Y.-H. Kim, and Y.-T. Kim, "An efficient neural network based indoor-outdoor scene classification algorithm," in *International Conference on Consumer Electronics*, 2010, pp. 317–318.

TABLE 3
Comparison of running times of our approach, the brute force and the generalised SMAWK algorithms. Speedup shows the speedup of our approach w.r.t. alternative approaches.

C	N	Ours	Brute Force	Speedup	SMAWK	Speedup
2	256	$14.788\ \mu s$	$4,795\ \mu s$	324	$4,608\ \mu s$	312
2	$65,536$	$2.636\ ms$	$207,453\ ms$	$78,700$	$302,362\ ms$	$114,705$
3	256	N/A	$387.710\ ms$	N/A	$17.661\ ms$	N/A
3	$65,536$	N/A	>24 hours	N/A	$1,115.462\ s$	N/A

[30] A. Savakis, "A computationally efficient approach to indoor/outdoor scene classification," in *Int. Conf. Pattern Recognition ICPR*, 2002, pp. vol. 4: 146–149.

[31] J. Wu and J. M. Rehg, "Centrist: A visual descriptor for scene categorization," *IEEE Trans. PAMI*, vol. 33, no. 8, pp. 1489–1501, 2011.

[32] R. M. Haralick, "Statistical and structural approaches to texture," *Proc. IEEE*, vol. 67, no. 5, pp. 786–804, 1979.

[33] P. L. Rosin and Y.-K. Lai, "Artistic minimal rendering with lines and blocks," *Graphical Models*, vol. 75, no. 4, pp. 208–229, 2013.

[34] H. Kang, S. Lee, and C. K. Chui, "Coherent line drawing," in *ACM Symp. Non-photorealistic Animation and Rendering*, 2007, pp. 43–50.

[35] A. Meijster and M. Wilkinson, "A comparison of algorithms for connected set openings and closings," *IEEE Trans. PAMI*, vol. 24, no. 4, pp. 484–494, 2002.

[36] S. Ali, M. Shah, and M. Shah, "Floor fields for tracking in high density crowd scenes." in *Europ. Conf. Computer Vision*, vol. 2, 2008, pp. 1–14.

[37] C.-C. Chang and C.-J. Lin, "LIBSVM: A library for support vector machines," *ACM Transactions on Intelligent Systems and Technology*, vol. 2, no. 3, pp. 27:1–27:27, 2011.

APPENDIX

We now give the proofs for the theorem and corollaries that allow the efficient thresholding algorithm.

Lemma A.1. *Consider a portion of a circular histogram $i..j$ (inclusive) with $i \leq j$. The mean $\mu = \frac{\sum_{x=i}^{j} xp(x)}{\sum_{x=i}^{j} p(x)}$ is the unique minimiser of $\sum_{x=i}^{j} p(x)(x-x^*)^2$, i.e. $\mu = \arg\min_{x^*} \sum_{x=i}^{j} p(x)(x-x^*)^2$ (assuming $\sum_{x=i}^{j} p(x) \neq 0$ otherwise the mean is undefined).*

Proof: Let $f(x^*) = \sum_{x=i}^{j} p(x)(x-x^*)^2$, then the minimum can be achieved with

$$\frac{\partial f}{\partial x^*} = 0. \tag{2}$$

This is equivalent to

$$2\sum_{x=i}^{j} p(x)(x^* - x) = 0. \tag{3}$$

$$\sum_{x=i}^{j} p(x)x^* = \sum_{x=i}^{j} xp(x) \tag{4}$$

So

$$x^* = \frac{\sum_{x=i}^{j} xp(x)}{\sum_{x=i}^{j} p(x)} = \mu. \tag{5}$$

□

The lemma gives an essential property that the mean of a histogram portion satisfies. The following corollary further shows that the property can be generalised to arbitrary circular histogram portions.

Corollary A.2. *Assume we define the circular sum $\mathring{\sum}_{x=i}^{j}$ as $\sum_{x=i}^{j}$ if $i \leq j$ and $\sum_{x=i}^{N} + \sum_{x=1}^{j}$ otherwise. We also define circular difference w.r.t. a starting position i as $a \mathring{-} b = (a-i) \mod N - (b-i) \mod N$, where $p \mod q$ gives a non-negative integer that has the remainder as p divided by q. This can be considered as measuring the difference after rotating the histogram such that i becomes the first element. Then $\mu = \arg\min_{x^*} \mathring{\sum}_{x=i}^{j} p(x)(x \mathring{-} x^*)^2$ is well defined for general circular histogram portions and is consistent with the mean of the linear histogram with appropriate rotation and this is hereafter defined as the mean of the circular histogram portion. If $\mathring{\sum}_{x=i}^{j} p(x) = 0$, any position x^* in the portion can be treated as μ as it is a minimiser of $\mathring{\sum}_{x=i}^{j} p(x)(x \mathring{-} x^*)^2$ and the following proofs still hold.*

Lemma A.3. *Consider two adjacent portions of a circular histogram $i..j-1$ and $j..k$ (both inclusive). Let μ_1 be the mean of $i..j-1$ and μ_2 be the mean of $j..k$. The total within-class variance is defined as*

$$\sigma^2 = \mathring{\sum}_{x=i}^{j-1} p(x)(x \mathring{-} \mu_1)^2 + \mathring{\sum}_{x=j}^{k} p(x)(x \mathring{-} \mu_2)^2 \tag{6}$$

Without loss of generality, assume $|j \mathring{-} \mu_1| \leq |\mu_2 \mathring{-} j|$. The total within-class variance with a different thresholding $i..j$ and $j+1..k$ is represented as $\bar{\sigma}^2$. Then we have $\bar{\sigma}^2 \leq \sigma^2$.

Proof: Let $\bar{\mu}_1$ and $\bar{\mu}_2$ represent the means of histogram portions $i..j$ and $j+1..k$, respectively.

$$\bar{\sigma}^2 = \mathring{\sum}_{x=i}^{j} p(x)(x \mathring{-} \bar{\mu}_1)^2 + \mathring{\sum}_{x=j+1}^{k} p(x)(x \mathring{-} \bar{\mu}_2)^2. \tag{7}$$

Using Lemma A.1 and the assumption $|j \mathring{-} \mu_1| \leq |\mu_2 \mathring{-} j|$:

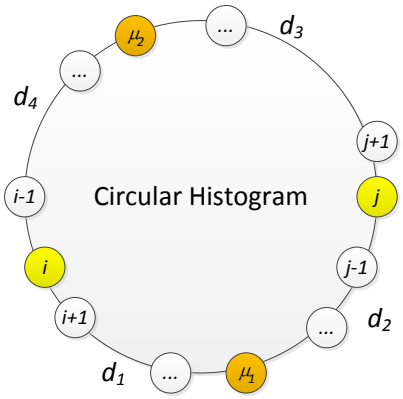

Fig. 9. Illustration for the proof of Theorem 2.1.

$$\begin{aligned}
\bar{\sigma}^2 &\leq \overset{\circ}{\sum}_{x=i}^{j} p(x)(x\overset{\circ}{-}\mu_1)^2 + \overset{\circ}{\sum}_{x=j+1}^{k} p(x)(x\overset{\circ}{-}\mu_2)^2 \\
&= \overset{\circ}{\sum}_{x=i}^{j-1} p(x)(x\overset{\circ}{-}\mu_1)^2 + p(j)(j\overset{\circ}{-}\mu_1)^2 \\
&\quad + \overset{\circ}{\sum}_{x=j+1}^{k} p(x)(x\overset{\circ}{-}\mu_2)^2 \\
&\leq \overset{\circ}{\sum}_{x=i}^{j-1} p(x)(x\overset{\circ}{-}\mu_1)^2 + p(j)(j\overset{\circ}{-}\mu_2)^2 \\
&\quad + \overset{\circ}{\sum}_{x=j+1}^{k} p(x)(x\overset{\circ}{-}\mu_2)^2 \\
&= \overset{\circ}{\sum}_{x=i}^{j-1} p(x)(x\overset{\circ}{-}\mu_1)^2 + \overset{\circ}{\sum}_{x=j}^{k} p(x)(x\overset{\circ}{-}\mu_2)^2 \\
&= \sigma^2. \qquad (8)
\end{aligned}$$

□

This lemma shows that for two adjacent circular histogram problems, if the distance from the mean of one portion to the shared end is smaller than the distance from the mean of the other portion to the shared end, then no worse solution can be obtained by moving one element from the second portion to the first. We obtain the similar conclusion in the opposite scenario as the following corollary:

Corollary A.4. *With the same assumption as Lemma A.3, but change* $|j\overset{\circ}{-}\mu_1| \leq |\mu_2\overset{\circ}{-}j|$ *to* $|(j-1)\overset{\circ}{-}\mu_1| \geq |\mu_2\overset{\circ}{-}(j-1)|$*, define* $\bar{\sigma}^2$ *as the total within-class variance of* $i..j-2$ *and* $j-1..k$*, then* $\bar{\sigma}^2 \leq \sigma^2$*.*

The following lemma considers the necessary and sufficient condition to have the mean unchanged when a new element is added to the histogram portion.

Lemma A.5. *For a portion of histogram* $i..j+1$ *(inclusive), the mean* $\mu_{i..j} = \mu_{i..j+1}$ *iff* $p(j+1) = 0$ *(assuming* $\overset{\circ}{\sum}_{x=i}^{j} p(x) \neq 0$ *as otherwise* $\mu_{i..j}$ *is not well defined).*

Proof: Since the mean of a circular portion rotates along with the circular portion, it is sufficient to show that this holds when the circular portion does not cross the end of the linearised histogram. Using Lemma A.1,

$$\begin{aligned}
& \mu_{i..j} = \mu_{i..j+1} \\
\Leftrightarrow \quad & \frac{\sum_{x=i}^{j} xp(x)}{\sum_{x=i}^{j} p(x)} = \frac{\sum_{x=i}^{j} xp(x) + (j+1)p(j+1)}{\sum_{x=i}^{j} p(x) + p(j+1)} \\
\Leftrightarrow \quad & p(j+1)\sum_{x=i}^{j} xp(x) = p(j+1)(j+1)\sum_{x=i}^{j} p(x). \qquad (9)
\end{aligned}$$

The last equation holds when either $p(j+1) = 0$ or $\sum_{x=i}^{j} xp(x) = (j+1)\sum_{x=i}^{j} p(x)$. Since $\sum_{x=i}^{j} p(x) \neq 0$, $\exists x,\ p(x) > 0$, so

$$\begin{aligned}
p(j+1)\sum_{x=i}^{j} xp(x) &< p(j+1)\sum_{x=i}^{j}(j+1)p(x) \\
&= p(j+1)(j+1)\sum_{x=i}^{j} p(x). \qquad (10)
\end{aligned}$$

□

Corollary A.6. *If* $p(x) > 0, \forall x$*, then* $\mu_{i..j} \neq \mu_{i..j+1}$*.*

Corollary A.7. *If* $p(x) > 0, \forall x$*, in addition to the assumptions in Lemma A.3 (or Corollary A.4), then* $\bar{\sigma}^2 < \sigma^2$*.*

This shows the condition that the previous inequalities are strictly satisfied. Based on the lemmas and corollaries discussed so far, the following theorem states the property that an optimal solution to the circular thresholding based on σ_W^2 satisfies. This is essential to the efficient algorithm.

Theorem 2.1. *For a circular histogram of length* $N = 2n$*, applying the two-class Otsu criterion (*σ_W^2*) using linear statistics extending to circular histograms, assume the best answer is* $i..j-1,\ j..i-1$*. Then, there exists a best solution, such that* $|j\overset{\circ}{-}i| = n$*. (Note that the starting position for* $\overset{\circ}{-}$ *in this case does not matter as the distance happens to be half of* N*.)*

Proof: We treat i as the starting point for $\overset{\circ}{-}$ in the following to avoid crossing the end. This is equivalent to rotating the histogram such that it starts from i.

Let μ_1 and μ_2 be the means of circular portions $i..j-1$ and $j..i-1$. If the best solution has $|j\overset{\circ}{-}i| = n$ (i.e. two portions each with n elements) then this is proved.

Otherwise, without loss of generality, assume $|j\overset{\circ}{-}i| \leq n-1$, so $j..i-1$ has at least $n+1$ elements.

As illustrated in figure 9, let $d_1 = |\mu_1\overset{\circ}{-}(i-1)|$, $d_2 = |j\overset{\circ}{-}\mu_1|$, $d_3 = |\mu_2\overset{\circ}{-}j|$ and $d_4 = |(i-1)\overset{\circ}{-}\mu_2|$. If $d_2 \leq d_3$ then according to Lemma A.3, a best solution can be obtained by moving an element from $j..i-1$ to $i..j-1$ thus reducing the length difference between two segments.

Similarly if $d_1 \leq d_4$, then a best solution can also be obtained by moving an element from $j..i-1$ to

$i..j-1$ thus reducing the length difference between two segments.

Otherwise, we have $d_1 + d_2 > d_3 + d_4$, however $d_1 + d_2 \leq n$ and $d_3 + d_4 \geq n$, so this is impossible.

So as long as $|j \dot{-} i| \leq n-1$ holds, elements can be kept moving from $j..i-1$ to $i..j-1$ until both have the same number of elements. □

The following corollaries further consider the cases where N is an odd number, and when the optimal solution is unique.

Corollary 2.2. *If $p(x) > 0, \forall x$, then the* unique *best solution has each segment containing n elements.*

Corollary 2.3. *If the length of the histogram $N = 2n+1$, then there exists a best solution such that one segment contains n elements and the other contains $n+1$ elements. Moreover, if $p(x) > 0, \forall x$, then the* unique *best solution satisfies that one segment has n elements and the other has $n+1$ elements.*